Acta Pharmaceutica Sinica B 2025;15(2):692−706

Chinese Pharmaceutical Association
Institute of Materia Medica, Chinese Academy of Medical Sciences

Acta Pharmaceutica Sinica B

www.elsevier.com/locate/apsb
www.sciencedirect.com

ORIGINAL ARTICLE

Enhanced radiotheranostic targeting of integrin $\alpha5\beta1$ with PEGylation-enabled peptide multidisplay platform (PEGibody): A strategy for prolonged tumor retention with fast blood clearance

Siqi Zhang [a,†], Xiaohui Ma [d,†], Jiang Wu [e,†], Jieting Shen [a], Yuntao Shi [a], Xingkai Wang [a], Lin Xie [b], Xiaona Sun [a], Yuxuan Wu [a], Hao Tian [a], Xin Gao [a], Xueyao Chen [a], Hongyi Huang [a], Lu Chen [a], Xuekai Song [a], Qichen Hu [a], Hailong Zhang [f], Feng Wang [e,*], Zhao-Hui Jin [c,*], Ming-Rong Zhang [b,*], Rui Wang [a,f,*], Kuan Hu [a,b,*]

[a]*State Key Laboratory of Bioactive Substance and Function of Natural Medicines, Institute of Materia Medica, Chinese Academy of Medical Sciences and Peking Union Medical College, Beijing 100050, China*
[b]*Department of Advanced Nuclear Medicine Sciences, Institute for Quantum Medical Science, National Institutes for Quantum Science and Technology (QST), Chiba 263-8555, Japan*
[c]*Department of Molecular Imaging and Theranostics, Institute for Quantum Medical Science, National Institutes for Quantum Science and Technology (QST), Chiba 263-8555, Japan*
[d]*Department of Vascular and Endovascular Surgery, the First Medical Center of Chinese PLA General Hospital, Beijing 100853, China*
[e]*Department of Nuclear Medicine, Nanjing First Hospital, Nanjing Medical University, Nanjing 211166, China*
[f]*Key Laboratory of Preclinical Study for New Drugs of Gansu Province, School of Basic Medical Sciences & Research Unit of Peptide Science, Chinese Academy of Medical Sciences, Lanzhou University, Lanzhou 730000, China*

Received 4 March 2024; received in revised form 29 May 2024; accepted 1 July 2024

*Corresponding authors.
E-mail addresses: fengwangcn@njmu.edu.cn (Feng Wang), jin.zhao-hui@qst.go.jp (Zhao-Hui Jin), zhang.ming-rong@qst.go.jp (Ming-Rong Zhang), wangrui@lzu.edu.cn (Rui Wang), hukuan@imm.ac.cn (Kuan Hu).
[†]These authors made equal contributions to this work.
Peer review under the responsibility of Chinese Pharmaceutical Association and Institute of Materia Medica, Chinese Academy of Medical Sciences.

https://doi.org/10.1016/j.apsb.2024.07.006

KEY WORDS

Integrin $\alpha5\beta1$;
Peptide;
PET imaging;
Targeted radionuclide therapy;
PEGylation;
Tumor;
Multidisplay;
PEGibody

Abstract Peptide-based radiopharmaceuticals targeting integrin $\alpha5\beta1$ show promise for precise tumor diagnosis and treatment. However, current peptide-based radioligands that target $\alpha5\beta1$ demonstrate inadequate *in vivo* performance owing to limited tumor retention. The use of PEGylation to enhance the tumor retention of radiopharmaceuticals by prolonging blood circulation time poses a risk of increased blood toxicity. Therefore, a PEGylation strategy that boosts tumor retention while minimizing blood circulation time is urgently needed. Here, we developed a PEGylation-enabled peptide multidisplay platform (PEGibody) for PR_b, an $\alpha5\beta1$ targeting peptide. PEGibody generation involved PEGylation and self-assembly. [^{64}Cu]QM-2303 PEGibodies displayed spherical nanoparticles ranging from 100 to 200 nm in diameter. Compared with non-PEGylated radioligands, [^{64}Cu]QM-2303 demonstrated enhanced tumor retention time due to increased binding affinity and stability. Importantly, the biodistribution analysis confirmed rapid clearance of [^{64}Cu]QM-2303 from the bloodstream. Administration of a single dose of [^{177}Lu]QM-2303 led to robust antitumor efficacy. Furthermore, [^{64}Cu]/[^{177}Lu]QM-2303 exhibited low hematological and organ toxicity in both healthy and tumor-bearing mice. Therefore, this study presents a PEGibody-based radiotheranostic approach that enhances tumor retention time and provides long-lasting antitumor effects without prolonging blood circulation lifetime. The PEGibody-based radiopharmaceutical [^{64}Cu]/[^{177}Lu]QM-2303 shows great potential for positron emission tomography imaging-guided targeted radionuclide therapy for $\alpha5\beta1$-overexpressing tumors.

1. Introduction

Peptide-based radiopharmaceuticals are advantageous due to their remarkable capacity to achieve efficient cancer diagnosis and therapy[1−3]. The combination of positron emission tomography (PET)/single photon emission computed tomography (SPECT) imaging enables real-time monitoring of whole-body tumor status after radiotracer administration[4−6]. Moreover, the energy from radionuclides causes precise and direct cytotoxic radiation exposure and DNA damage, giving targeted radionuclide therapy (TRT) multiple advantages over conventional therapeutic modalities. As a result of their favorable pharmacokinetic and pharmacodynamic properties, as well as their ease of synthesis and chemical modification, peptides have become widely implemented as targeting ligands for the delivery of radionuclides to tumor cells[4,7,8]. Recently, US Food and Drug Administration-approved radiopharmaceuticals, including [^{177}Lu]/[^{68}Ga]DOTATATE[9,10], [^{68}Ga]PSMA-11 and [^{177}Lu]PSMA-617, have utilized peptides or peptidomimetics as targeting ligands[11−15]. The rapid growth of TRT has led to an increasing demand for peptide ligands with high recognition capacity for tumor targets and prolonged retention time in tumors to ensure long-acting antitumor effects[3,16−18].

Integrins are a family of heterodimeric cell receptors composed of an α subunit and a β subunit. They play essential roles in regulating cell adhesion, proliferation, differentiation, and migration through interactions with the extracellular matrix[19−23]. Eighteen α subunits and eight β subunits form twenty-four different integrins[24]. Integrin $\alpha5\beta1$, also known as the fibronectin receptor, is the only known $\alpha5$ integrin [25,26]. Multiple tumor types demonstrate high integrin $\alpha5\beta1$ expression, and its upregulation has been strongly associated with tumor proliferation, metastasis, and progression[27,28]. Therefore, integrin $\alpha5\beta1$ has emerged as a promising target for tumor diagnosis and therapy[20,21,29]. Several $\alpha5\beta1$-targeting peptide-based radiotracers have been developed, including the ^{68}Ga-labelling peptidomimetic and the ^{68}Ga-labelling *N*-methylated isoDGR peptide, both of which demonstrate high tumor uptake on PET imaging[30,31]. Additionally, [^{68}Ga]aquibeprin, a pseudopeptide-based radiotracer, has demonstrated greater binding affinity to the tumor integrin $\alpha5\beta1$ than to $\alpha v\beta3$[32,33]. However, radioligands with both high selectivity and durable retention that are compatible with radionuclide therapy for $\alpha5\beta1$-overexpressing tumors are still largely unavailable.

The integrin $\alpha5\beta1$-targeting peptide PR_b was designed by mimicking the binding epitope of fibronectin to $\alpha5\beta1$[34−40]. The dual-site recognition of PR_b makes it a remarkable ligand for $\alpha5\beta1$-selective radiotracer. ^{18}F-labeling PR_b has presented selective tumor uptake in integrin $\alpha5\beta1$-positive tumors but rapid degradation and short retention time in tumors, hampering its potential clinical utility, particularly for TRT[41]. Modification strategies that can enhance the *in vivo* stability while maintaining the high selectivity of PR_b are therefore needed.

Polyethylene glycol (PEG) modification is a commonly used strategy to enhance the tumor retention time of peptide-based radiopharmaceuticals[42−47]. A mechanistic study revealed that serum protein binding and proteolytic enzyme shielding were two dominant effects of PEG modification[48]. As a result, the modified peptides may exhibit a remarkably prolonged blood circulation lifetime, which is usually pursued in long-acting drugs for diabetes mellitus and weight loss. However, for radiopharmaceuticals, an extended circulation time in the blood increases blood radiation dosimetry, thus raising concerns about hematological toxicity. In this context, a new PEGylation strategy for peptide-based radiopharmaceuticals that can tumor retention time while minimizing blood residence time is urgently needed.

To address this issue, we proposed a PEGylation-enabled multidisplay platform, denoted as PEGibody, as a viable solution for developing safer and more effective $\alpha5\beta1$-targeting radiotheranostics. By harnessing a two-step process that integrates PEG conjugation and PEG-induced self-assembly, an $\alpha5\beta1$-binding peptide PR_b-derived PEGibody, namely [^{64}Cu]QM-2303, was generated, and the *in vitro* stability and binding affinity of the tracer were evaluated. Whole-body PET imaging and *ex vivo* biodistribution analysis were performed to evaluate its *in vivo*

performance. The antitumor efficacy of [^{177}Lu]QM-2303 was evaluated to demonstrate its potential in therapeutic practice.

2. Materials and methods

2.1. Reagents and materials

The reagents involved in solid-phase peptide synthesis and chelator conjugation were purchased from Sigma−Aldrich (St. Louis, MO, USA), MACKLIN (Shanghai, China), or Wako Pure Chemical Industries (Osaka, Japan). ^{64}Cu (98% radionuclidic purity) was produced in-house at the National Institutes for Quantum Science and Technology (Chiba, Japan). ^{177}Lu was purchased from DC AMS PHARMA (Nanjing, China) with 98% radionuclidic purity. All reagents for cell culture were obtained from Gibco (ThermoFisher Scientific, Waltham, MA, USA).

2.2. Tumor cell line culture and tumor-bearing mouse model establishment

We utilized the murine melanoma cell line B16F10 as the tumor cell model to evaluate the effects of radiotracers. The cells were cultured in Dulbecco's modified Eagle's medium (DMEM) with high glucose supplemented with 10% fetal bovine serum, 100 U/mL penicillin, and 50 μg/mL streptomycin. The medium was replaced with fresh medium every two days, and the cells were passaged when 80%−90% confluency was reached.

C57BL/6J and BALB/c nude mice (4−5 weeks old) were obtained from Japan SLC Ltd. (Shizuoka, Japan) and GemPharmatech (Beijing, China). We ensured that all animals received humane care, and the experiments were performed strictly according to the instructions of the Committee for the Care and Use of Laboratory Animals. The Animal Ethics Committee of the National Institutes of Quantum Science and Technology and Nanjing Medical University approved all the animal studies. To establish tumor-bearing mouse models, B16F10 cells were subcutaneously injected into the left flank of C57BL/6J and BALB/c nude mice (1×10^6 cells/mouse, 1 tumor/mouse). The growth of the tumor allografts was observed every two days. Generally, PET imaging was performed 10 days after transplantation.

2.3. Peptide synthesis and ^{64}Cu radiolabeling

PR_b was synthesized following the commonly used Fmoc-based solid-phase peptide synthesis method, as we previously described[49,50]. The sequence of PR_b is KSSPHSRNSGSGSGSG SGRGDSP. 1,4,7-Triazacyclononane-1,4,7-triacetic acid (NOTA) was conjugated to the N-terminus of PR_b to generate QM-2301 (Supporting Information Figs. S1 and S3). Insertion of a cysteine at the C-terminus of QM-2301 yielded QM-2302 (Supporting Information Fig. S2). For radionuclide labeling of QM-2301 and QM-2302, 20 μg precursor and $^{64}CuCl_2$ (350−400 MBq, 0.1 mol/L NaOAc, pH = 4.1) were coincubated for at least 10 min at 80 °C. To synthesize [^{64}Cu]QM-2303, QM-2302 was first PEGylated with 4-arm PEG molecules with a reaction duration of at least 6 h. The reaction mixture was then subjected to $^{64}CuCl_2$ labeling. The quality control parameters of [^{64}Cu]QM-2301, [^{64}Cu]QM-2302, and [^{64}Cu]QM-2303 were analyzed by radio-high-performance liquid chromatography (radio-HPLC; Shimadzu, Kyoto, Japan). The formation and size of the QM-2303-based PEGibody were determined by dynamic light scattering (DLS; Brookhaven, USA) assays and the Tyndall effect.

2.4. Transmission electron microscopy (TEM)

[^{nat}Cu]QM-2303 and PEG solution were loaded onto copper grids coated with a carbon film that was glow discharged for 1 min. The excess sample was removed with filter paper. Then, 2% uranyl acetate was used to stain samples and the samples were imaged by TEM (FEI Talos F200X, USA) at a voltage of 80 kV.

2.5. Radiotracer stability assay

To determine the *in vitro* stability, [^{64}Cu]QM-2301, [^{64}Cu]QM-2302, and [^{64}Cu]QM-2303 were incubated in murine serum at 37 °C with slight agitation for 30 or 60 min. The solutions were collected and analyzed by radio-HPLC with a C18 column.

2.6. Surface plasmon resonance (SPR) assay

Interactions between $\alpha5\beta1$ and the peptides were analyzed using a Biacore 8K system (Cytiva, MA, USA). Recombinant human integrin $\alpha5\beta1$ (alpha 5 beta 1, HY-P77718, MCE, NJ, USA) was immobilized on a CM5 sensor chip using a standard amine coupling kit at a temperature of 25 °C. The final immobilization level of $\alpha5\beta1$ was 5500−7500 RU. Peptides were injected as analytes at various concentrations in HBS-P running buffer (40 mmol/L HEPES buffer, 5.4 mmol/L NaCl, 274 mmol/L KCl, 2 mmol/L $MgCl_2$, 0.1% surfactant P20, pH 7.4) containing 5% dimethyl sulfoxide to evaluate the binding affinity. The chip platform contact time was 120 s, and the dissociation time was 240 s. The data was analyzed using Biacore evaluation software (8K version 1.0), fitted using a 1:1 steady affinity model and plotted using GraphPad Prism.

2.7. Cell uptake and binding inhibition assays

For the cell uptake assay, B16F10 cells cultured in 12-well plates were treated with [^{64}Cu]QM-2301, [^{64}Cu]QM-2302, or [^{64}Cu]QM-2303 at a final concentration of 750 kBq/mL per well. After 5, 20, 40, 60, and 80 min, 0.2 mol/L NaOH was used as the cell dissociation reagent for cell lysate collection. The radioactivity of the cell lysates was measured using an autogamma counter (WIZARD2 2480, PerkinElmer, MA, USA). For the binding inhibition assays, the anti-$\alpha5\beta1$ antibody (ab275977, Abcam, Cambridge, UK) was used as an inhibitor. Radiotracers (20 μCi/mL) and different concentrations of inhibitors were added to the B16F10 cells, which were incubated for 2 h at 37 °C. The radioactivity of the cell lysates was measured as described above.

2.8. Immunofluorescence and immunohistochemistry (IHC) staining of integrin $\alpha5\beta1$

B16F10 tumor allografts were sectioned at 10 μm and then fixed in 4% paraformaldehyde overnight at 4 °C. For immunofluorescence staining, the sections were treated with 0.1% Triton X-100 and then blocked in 3% bovine serum albumin (BSA) at room temperature (RT) for 2 h. The sections were treated with anti-$\alpha5\beta1$ primary antibody (clone BMA5, 1:100 dilution; Millipore, Temecula, CA, USA) overnight at 4 °C. After being washed with phosphate-buffered saline (PBS) three times, the sections were

incubated with a secondary antibody (1:100 dilution in PBS; Thermo Scientific, Rockford, IL, USA) for 1 h at RT. DAPI (1 μg/mL) was used to label the cell nucleus, and the stained tissues were observed under a confocal fluorescence microscope.

For IHC staining, the sections were treated with 3% H_2O_2 after penetration in Triton-X100. Then the sections were incubated with primary and secondary antibodies as described above. DAB Horseradish Peroxidase Color Kit (Beyotime, P0202, Shanghai, China) was then used to visualize the expression of integrin $\alpha5\beta1$. The cell nucleus were stained using hematoxylin reagent following the standard method.

2.9. Flow cytometry assay

The expression of integrin $\alpha5\beta1$ in B16F10 cells was confirmed by flow cytometry, as previously reported[41]. The B16F10 cells were treated with 0.25% trypsin−EDTA at 37 °C for 1 min to detach the cells. The cells were then treated with rat anti-mouse primary antibody against the $\alpha5$ subunit (clone 5H10-27, 1:100 dilution; BD Biosciences, Franklin Lakes, NJ, USA), the $\beta1$ subunit (clone KM16, 1:100 dilution; eBioscience, San Diego, CA, USA), or $\alpha5\beta1$ (clone BMA5, 1:100 dilution; Millipore, Temecula, CA, USA), respectively, or with antibody diluent only (PBS containing 1% BSA and 1 mmol/L $CaCl_2$). The cells were subsequently stained with fluorescein-conjugated goat anti-rat IgG secondary antibody (1:100 dilution, Thermo Scientific, Rockford, IL, USA) and analyzed by flow cytometry using a Guava system (Guava Technologies-Millipore, Hayward, CA, USA).

2.10. Western blotting analysis

The B16F10 cells were treated with RIPA lysis buffer (Beyotime, P0013B, Shanghai, China) for cell lysate collection. After centrifuging at 12,000 rpm for 20 min, the supernatant was collected. The total protein concentration was determined using a BCA Protein Assay Kit (Beyotime, P0009, Shanghai, China). For Western blotting, the cell lysate was electrophoresed on 8% SDS−PAGE for 20 min, followed by 200 V for 30 min. Then, the protein was transferred to a polyvinylidene difluoride (PVDF) membrane for 2 h at 4 °C. After transferring, 5% skimmed milk was added to the PVDF membrane for blocking over 3 h in a shaker at RT. Primary antibodies against integrin $\alpha5$ (ab150361, 1:5000; Abcam, Cambridge, UK) and integrin $\beta1$ (sc-374429, 1:100; Santa Cruz, TX, USA) were added and incubated overnight at 4 °C with agitation. After washing with 1% TBST three times, the PVDF membrane was incubated with secondary antibody for 1 h at RT. Finally, the immunoblots were visualized with enhanced chemiluminescence solution.

2.11. Small animal PET/CT imaging

PET imaging was performed when the B16F10 tumors reached at least 100 mm^3 [^{64}Cu]QM-2301, [^{64}Cu]QM-2302, or [^{64}Cu]QM-2303 (200 μCi in 100 μL normal saline) were injected into each mouse *via* the tail vein. Inveon Micro-PET/CT (Siemens Medical Solutions, Knoxville, Munich, Germany) was used for the PET/CT scans. The dynamic PET/CT scans were performed immediately after injection and lasted for 1 h (three mice for each radiotracer). For [^{64}Cu]QM-2303, static scans were performed at 0.5, 1, 5, 10, and 24 h post-injection (p.i.). The analysis of PET/CT data was performed at the Inveon Research Workstation with the decay correction of radioactivity. The uptake levels of radiotracers in tumors and organs of interest are presented as percentage of the injected dose per gram (%ID/g).

2.12. Ex vivo biodistribution assays

For the *ex vivo* biodistribution experiments, B16F10 tumor-bearing mice were injected with [^{64}Cu]QM-2301, [^{64}Cu]QM-2302, or [^{64}Cu]QM-2303 (100 μCi in 100 μL normal saline per mouse). For each time point (0.5, 1, 4, 24 h p.i.), at least three mice were executed and dissected to collect the tumors, blood samples, and major organs (brain, heart, lung, liver, spleen, pancreas, stomach, large intestine, small intestine, kidney, muscle, bone, skin, bladder, testis). After being wet weighed, each sample was then applied to an autogamma counter (as described above) for determination of the radioactivity, which was presented as % ID/g.

2.13. In vivo safety assessment of [^{64}Cu]QM-2303

For the safety assessment of [^{64}Cu]QM-2303, healthy C57BL/6J mice were injected with vehicle (100 μL normal saline per mouse) or [^{64}Cu]QM-2303 (3 mCi in 100 μL normal saline per mouse) through the tail vein. The body weights of the mice were measured before and after injection to determine the toxicity of the injection. Then, fresh blood was harvested through the tail vein for hematological analyses. The major organs, including the heart, liver, spleen, lungs, and kidneys, were collected at 30 days p.i. Following fixation in 4% paraformaldehyde and embedded in paraffin, hematoxylin and eosin (H&E) staining was performed to analyze the pathological lesions.

2.14. Therapeutic efficacy assessment

Synthesis and radiolabeling of [^{177}Lu]QM-2301 and [^{177}Lu]QM-2303 were performed according to the previously reported method[51]. The radiochemical purity of both was analyzed by radio-HPLC after filtration through a Sep-Pak™ Plus Short C18 column (WAT020515, Waters Corp., MA, USA). A single dose of [^{177}Lu]QM-2301 (500 μCi) or [^{177}Lu]QM-2303 (500 μCi) was intravenously injected into B16F10 tumor-bearing mice when the tumors reached at least 50 mm^3 ($n = 6$). Tumor volume and body weight were measured every 2 days. The tumor allografts were collected and analyzed by H&E staining. The major organs, including the heart, liver, spleen, lung, and kidney, were harvested 28 days after injection. H&E staining was performed to evaluate the pathological lesions. Blood samples were collected for hematology, liver, and kidney function analysis.

2.15. Statistical analysis

All quantitative data was presented as the mean ± standard deviation (SD) of at least three independent experiments. The statistical analysis was conducted using GraphPad Prism 8.0.1 software. The two-tailed, unpaired Student's *t*-test was used for two-group comparisons. Statistical significance is indicated as $^*P < 0.05$, $^{**}P < 0.01$, or $^{***}P < 0.001$.

3. Results

3.1. Synthesis and radiolabeling of [^{64}Cu]QM-2301, [^{64}Cu]QM-2302, and [^{64}Cu]QM-2303

PEGylation was used as a strategy to enhance the stability of QM-2301 (NOTA-conjugated PR_b). To accomplish this, the C-terminus cysteine-modified QM-2301, denoted as QM-2302 (Fig. S3), was obtained with a thiol group acting as a prosthetic group to link the peptide and PEG molecules. For [^{64}Cu]QM-2301 and [^{64}Cu]QM-2302, ^{64}Cu ($t_{1/2}$ = 12.7 h) radiolabeling achieved a high radiochemical yield (RCY >99%) and radiochemical purity (>99%), as confirmed by radio-HPLC analysis. [^{64}Cu]QM-2301 exhibited a retention time of approximately 6.54 min, while [^{64}Cu]QM-2302 was more hydrophilic, with a retention time of 5.80 min (Supporting Information Fig. S4A and S4B, Table 1). After synthesis, both tracers had a specific activity of at least 74 GBq/μmol (Table 1).

PEGylated QM-2303 was obtained by mixing QM-2302 with 4-arm PEG (Fig. 1A). Covalent conjugation of 4-arm PEG molecules and QM-2302 achieved a yield of 58.2% (calculated by QM-2302) at 6 h and even after a prolonged reaction time (Fig. 1B). Then, the QM-2303 mixture was subjected to ^{64}Cu labeling to generate the PEGibody [^{64}Cu]QM-2303 (Fig. 1A). Radio-HPLC analysis showed that [^{64}Cu]QM-2303 was obtained with a retention time of 8.69 min (Fig. 1C, Fig. S4C). The activity of the purified [^{64}Cu]QM-2303 was at least 30 GBq/μmol after synthesis (Table 1).

The morphology of the PEGibody [^{nat}Cu]QM-2303 was assessed. TEM and Tyndall effect assays revealed the formation of spherical nanoparticles with diameters ranging from 100 to 200 nm, consistent with the DLS data (Fig. 1D and E). Additionally, DLS revealed that [^{nat}Cu]QM-2303 was larger than the PEG molecules, further suggesting the linking of QM-2302 to PEG molecules (Fig. 1F). These results demonstrated that PEGylation induced QM-2302 self-assembly and yielded PEGibody.

3.2. In vitro characterization of [^{64}Cu]QM-2301, [^{64}Cu]QM-2302, and [^{64}Cu]QM-2303

We assessed the binding of QM-2301, QM-2302, and QM-2303 to recombinant human integrin $\alpha5\beta1$ by SPR. QM-2301 exhibited a mean equilibrium dissociation constant (K_D) of 1.44 ± 0.19 nmol/L. Higher binding affinities were observed for QM-2302 and QM-2303, with K_D values of 0.55 ± 0.08 and 0.21 ± 0.06 nmol/L, respectively. A seven-fold improvement in K_D was achieved after PEGylation, which may be attributed to the multivalent binding effects caused by the dense multidisplay of PR_b peptides on the surface of the PEGibody. Additionally, QM-2302 had a lower K_D than QM-2301, indicating that a cysteine modification enhanced the binding affinity (Fig. 2A and B). Based on these results, we proposed that the QM-2301 or QM-2302 monomer peptide binded to one integrin $\alpha5\beta1$ receptor, while the multivalent molecule PEGibody, QM-2303, enables multisite recognition, resulting in enhanced binding ability (Fig. 2C and D).

The murine melanoma B16F10 cell line was used to evaluate the *in vitro* behavior of the three radioligands. Flow cytometry, Western blotting, and immunofluorescence staining indicated high expression of integrin $\alpha5\beta1$ in B16F10 cells and tumor tissues (Fig. 2E and F, Supporting Information Fig. S5). The stability of the radioligands in murine serum was evaluated. Radio-HPLC revealed that 88% of [^{64}Cu]QM-2303 remained intact after 1 h of incubation with murine serum, which was in stark contrast to the approximately 38% of [^{64}Cu]QM-2301 and [^{64}Cu]QM-2302 that remained intact under the same conditions (Fig. 2G). These findings highlight the superior *in vivo* stability of [^{64}Cu]QM-2303 compared to [^{64}Cu]QM-2301 and [^{64}Cu]QM-2302.

The cell uptake of [^{64}Cu]QM-2301, [^{64}Cu]QM-2302, and [^{64}Cu]QM-2303 was time-dependent, with [^{64}Cu]QM-2303 demonstrating a greater percentage of binding to integrin $\alpha5\beta1$ than [^{64}Cu]QM-2301 and [^{64}Cu]QM-2302 (Fig. 2H). To confirm the binding specificity, we also performed a competitive binding experiment using B16F10 cells. The half-maximal inhibitory concentrations (IC_{50}) of [^{64}Cu]QM-2301 and [^{64}Cu]QM-2302 for the integrin $\alpha5\beta1$ inhibitor were 1.94 and 1.55 μmol/L respectively. Notably, a lower IC_{50} of 1.30 μmol/L was observed for [^{64}Cu]QM-2303, indicating that PEGylation improved the specific binding affinity for integrin $\alpha5\beta1$ (Fig. 2I). Taken together, these data suggest that the PEGibody-based radioligand [^{64}Cu]QM-2303 exhibited enhanced cellular uptake and stability.

3.3. In vivo PET/CT imaging of [^{64}Cu]QM-2301, [^{64}Cu]QM-2302, and [^{64}Cu]QM-2303 in healthy and tumor-bearing mice

To evaluate the *in vivo* pharmacokinetics of [^{64}Cu]QM-2301, [^{64}Cu]QM-2302, and [^{64}Cu]QM-2303, we performed PET/CT imaging of these radioligands in healthy mice. The PET/CT images obtained at various time points were analyzed to monitor the distribution of the tracers. [^{64}Cu]QM-2302 exhibited significantly increasing uptake in the kidney (>10 %ID/g) and bladder of mice during the early stage after injection, as confirmed by PET/CT imaging and time−activity curves (Fig. 3). Furthermore, the [^{64}Cu]QM-2303 signal decreased over time, while the liver signal increased, suggesting delayed clearance and a transition from kidney to hepatobiliary excretion. Importantly, no obvious accumulation of either radiotracer was detected in the other major organs.

We next evaluated the *in vivo* performance of [^{64}Cu]QM-2301, [^{64}Cu]QM-2302, and [^{64}Cu]QM-2303 in B16F10 tumor-bearing mice by PET/CT imaging. Dynamic PET/CT images

Table 1 Radiocharacteristics of [^{64}Cu]QM-2301, [^{64}Cu]QM-2302 and [^{64}Cu]QM-2303.

Tracer	[^{64}Cu]QM-2301	[^{64}Cu]QM-2302	[^{64}Cu]QM-2303
Retention time (min)	6.54	5.80	8.69
Radiochemical yield (%)	>99	>99	≈57
Specific activity (GBq/μmol)	>74 ± 10	>74 ± 10	>30 ± 10
Radiochemical purity (%)	>98	>98	>95
Chelator	NOTA	NOTA	NOTA

NOTA: 1,4,7-triazacyclononane-1,4,7-triacetic acid.
The retention time was determined by HPLC with the conditions as follows: column, YMC-Triat-C18 column (4.6 mm i.d. × 150 mm, 5 μm); solvent gradient, 10%−90% acetonitrile (0.1% trifluoroacetic acid (TFA)), 20 min; flow rate, 1 mL/min.

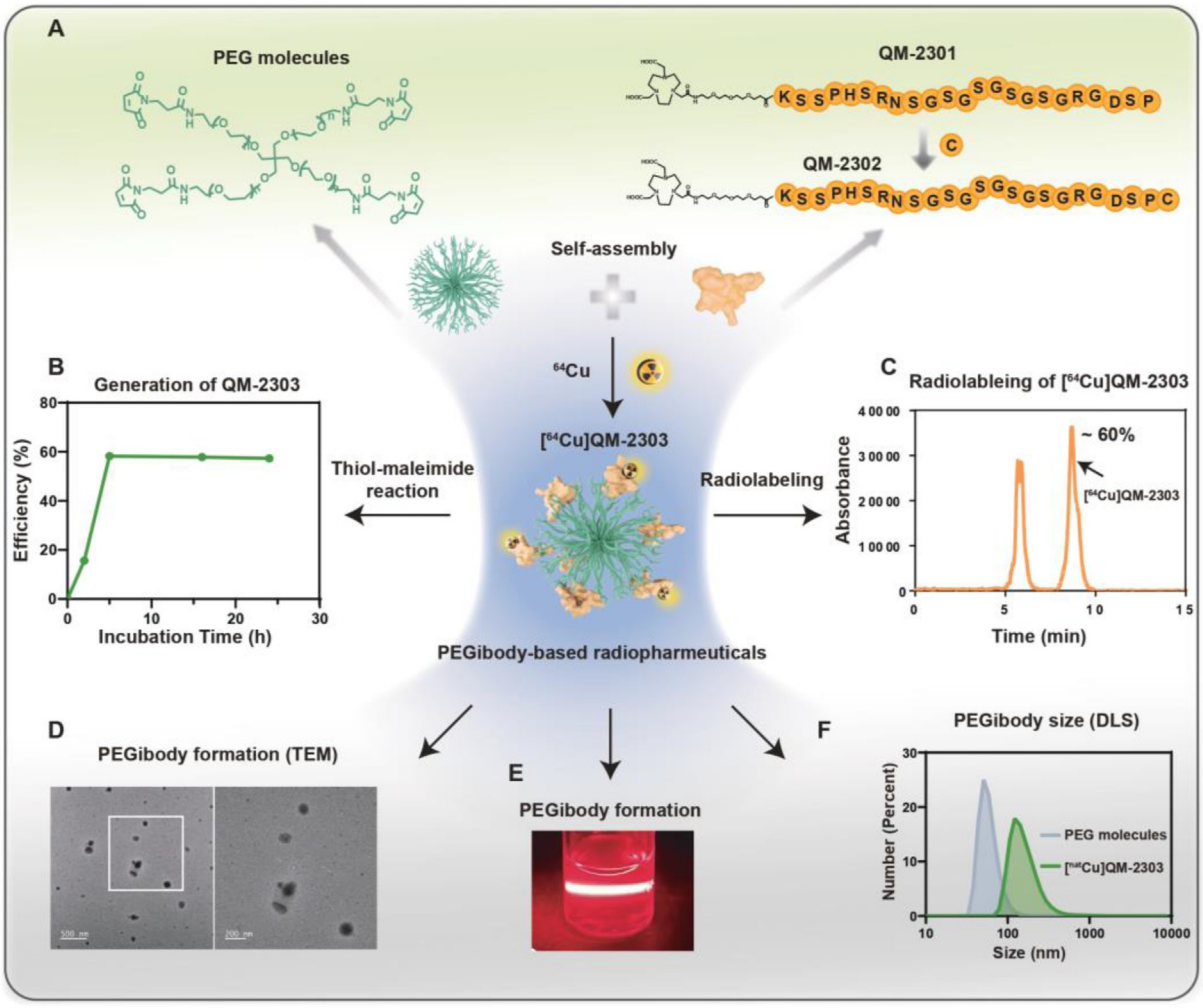

Figure 1 Synthesis and characterization of [^{64}Cu]QM-2303. (A) The chemical structures of the QM-2301, QM-2302, and 4-arm PEG molecules. Adding a cysteine at the C-terminus of QM-2301 yielded QM-2302. 4-arm PEG molecules self-assembled to form a PEGibody, which was subsequently PEGylated with QM-2302. The radiolabeling of ^{64}Cu or ^{177}Lu was then performed to generate the PEGibody-based radiopharmaceuticals. (B) The synthesis efficiency of PEGylated QM-2303 at different incubation times. QM-2302 and PEG were mixed for at least 6 h to reach a conversion efficiency of 58.2%. (C) A one-pot method for synthesis of [^{64}Cu]QM-2303 reached a yield of approximately 60%. (D) TEM images of QM-2303 showing the size of the PEGibody. Magnified images of the white box (right) suggest that QM-2303 forms uniform PEGibodies. Scale bars indicate 500 nm (left) and 200 nm (right). (E) The Tyndall effect of QM-2303 indicated the formation of PEGibodies. (F) DLS analysis of PEG molecules alone and PEGibody ([^{nat}Cu]QM-2303). PEGylated QM-2303 was self-assembled into a PEGibody with a size of 100−200 nm, which was larger than that of PEG molecules alone.

demonstrated significant tumor uptake of [^{64}Cu]QM-2301 and [^{64}Cu]QM-2302 at 30 min p.i. However, the tumor uptake of both radioligands rapidly decreased from 30 to 60 min p.i (Fig. 4A and B). The time−activity curves of tumor uptake during the initial 60 min also revealed a rapid decrease in radioactivity, which was barely detectable at 60 min p.i (Fig. 4D and Supporting Information Fig. S6A). Furthermore, a similar tendency of kidney uptake for [^{64}Cu]QM-2301 and [^{64}Cu]QM-2302 was observed, showing a gradual increase in the kidneys from 0 to 60 min p.i (Fig. 4D and Fig. S6A). The limited tumor accumulation and retention time of [^{64}Cu]QM-2301 and [^{64}Cu]QM-2302 may be due to the poor stability and low binding ability of radioligands *in vivo* (Fig. 4E).

To examine whether PEGibody increased tumor uptake *in vivo*, PET/CT imaging of [^{64}Cu]QM-2303 in B16F10 tumor-bearing mice was performed. Tumor accumulation of [^{64}Cu]QM-2303 was detected in the B16F10 tumor allografts immediately 0.5 h p.i. (Fig. 4C, and Fig. S6A). Notably, 1.26 %ID/g of [^{64}Cu]QM-2303 was retained in the tumor 1 h p.i., compared to 0.51 %ID/g of [^{64}Cu]QM-2302 and 0.35 %ID/g of [^{64}Cu]QM-2301 (Fig. 4C, D and Fig. S6B). Additionally, the tumor uptake of [^{64}Cu]QM-2303 was 1.5 %ID/g at 18 h p.i. and 1.0 % ID/g at 24 h p.i. (Fig. 4D and Fig. S6A). The time−activity curves of tumor uptake for [^{64}Cu]QM-2301, [^{64}Cu]QM-2302, and [^{64}Cu]QM-2303 further indicated a significantly prolonged retention time in the tumor sites of [^{64}Cu]QM-2303 (Fig. 4D). Moreover, the major organ accumulation of the radioligands was analyzed (Fig. 4D and Fig. S6). Notably, kidney accumulation of [^{64}Cu]QM-2303 was comparable to that of [^{64}Cu]QM-2301 at 0.5 and 1 h p.i. Overall, *in vivo* PET/CT imaging demonstrated that the PEGibody

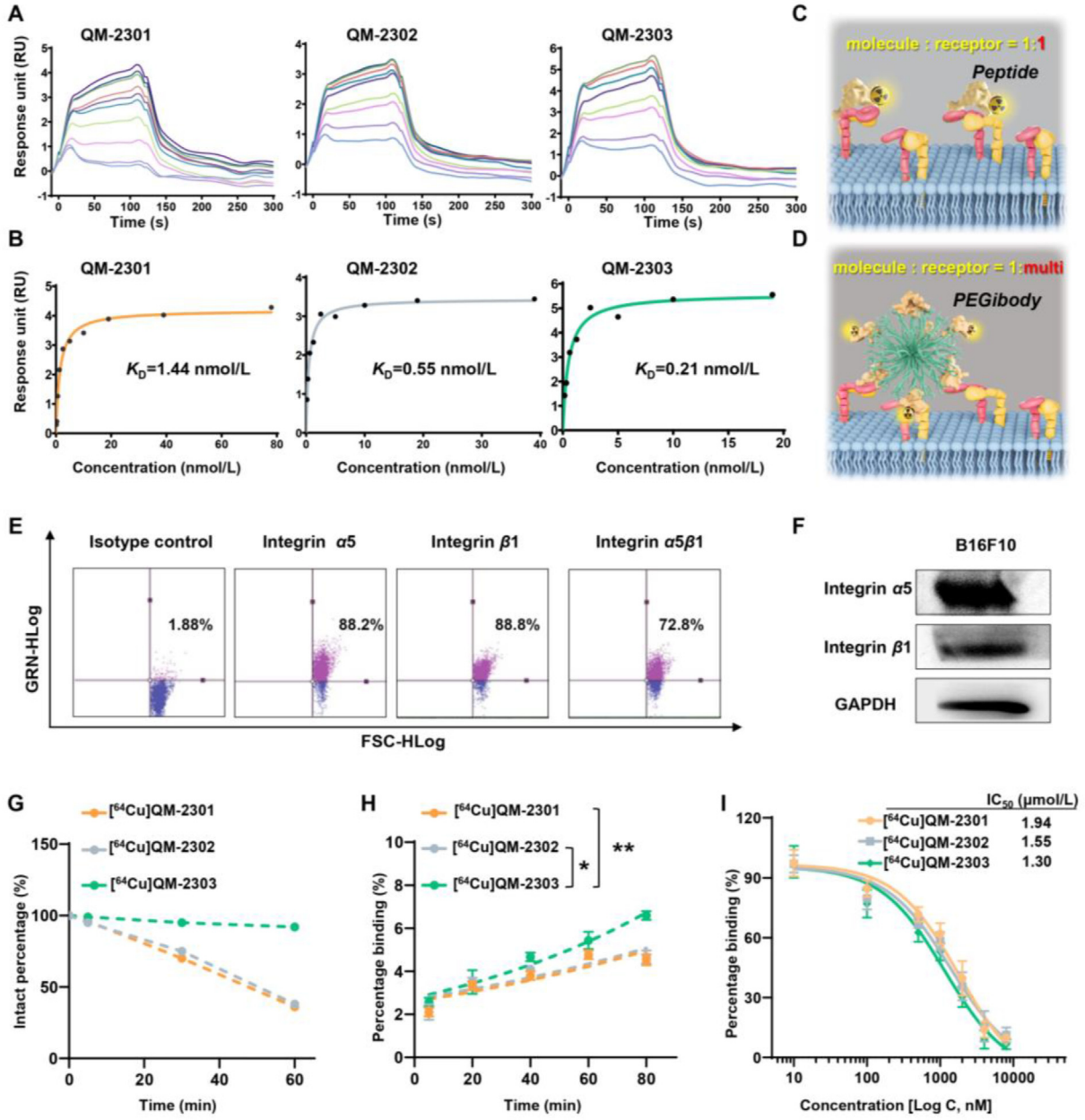

Figure 2 *In vitro* binding affinity and stability studies of [^{64}Cu]QM-2301, [^{64}Cu]QM-2302, and [^{64}Cu]QM-2303. (A) SPR sensorgrams demonstrating the binding affinity of QM-2301, QM-2302, and QM-2303 for human integrin $\alpha5\beta1$ in a concentration-dependent manner. (B) The equilibrium dissociation constant (K_D) of each peptide was calculated based on SPR measurements. The K_D values of each precursor are shown. (C, D) Schematic diagram of the binding patterns of [^{64}Cu]QM-2301, [^{64}Cu]QM-2302 (C), and [^{64}Cu]QM-2303 (D) to integrin $\alpha5\beta1$. Monomeric [^{64}Cu]QM-2301, and [^{64}Cu]QM-2302 bind to receptors in a single-network pattern. For [^{64}Cu]QM-2303, the PEGibody-based radiotracer, one PEGibody can bind to more than two integrin $\alpha5\beta1$ receptors, exhibiting better binding affinity. (E, F) The expression of integrin $\alpha5\beta1$ in B16F10 cells was analyzed by flow cytometry (E) and Western blotting (F). For flow cytometry assays, an anti-integrin $\alpha5 + \beta1$ antibody was used. For Western blot assays, integrin $\alpha5$ ($\sim$150 kDa) and integrin $\beta1$ ($\sim$138 kDa) were examined using two antibodies. (G) The stability of [^{64}Cu]QM-2301, [^{64}Cu]QM-2302, and [^{64}Cu]QM-2303 after coincubation with mouse serum within 1 h, as indicated by radio-HPLC. (H) *In vitro* cell uptake of [^{64}Cu]QM-2301, [^{64}Cu]QM-2302, and [^{64}Cu]QM-2303 (750 KBq/mL) when incubated with B16F10 cells for different time period. (I) IC_{50} of [^{64}Cu]QM-2301, [^{64}Cu]QM-2302, and [^{64}Cu]QM-2303 when inhibited with antibodies at different concentrations. $^*P < 0.05$, $^{**}P < 0.01$. All the quantitative experiments were performed independently at least three times (data are the mean $\pm$ SD, $n = 3$).

improved tumor uptake and retention without increasing the kidney burden.

PEG molecules may self-assemble and encapsulate the non-PEGylated monomer [^{64}Cu]QM-2302, enhancing its *in vivo* stability and tumor uptake. To investigate whether the increased tumor retention resulted from noncovalent PEG molecules, we performed PET imaging of a mixture containing PEG molecules and [^{64}Cu]QM-2302 monomers without conjugation after injection into B16F10 tumor-bearing mice. Compared with the [^{64}Cu]QM-2302_PEG mixtures, the [^{64}Cu]QM-2303 mixtures

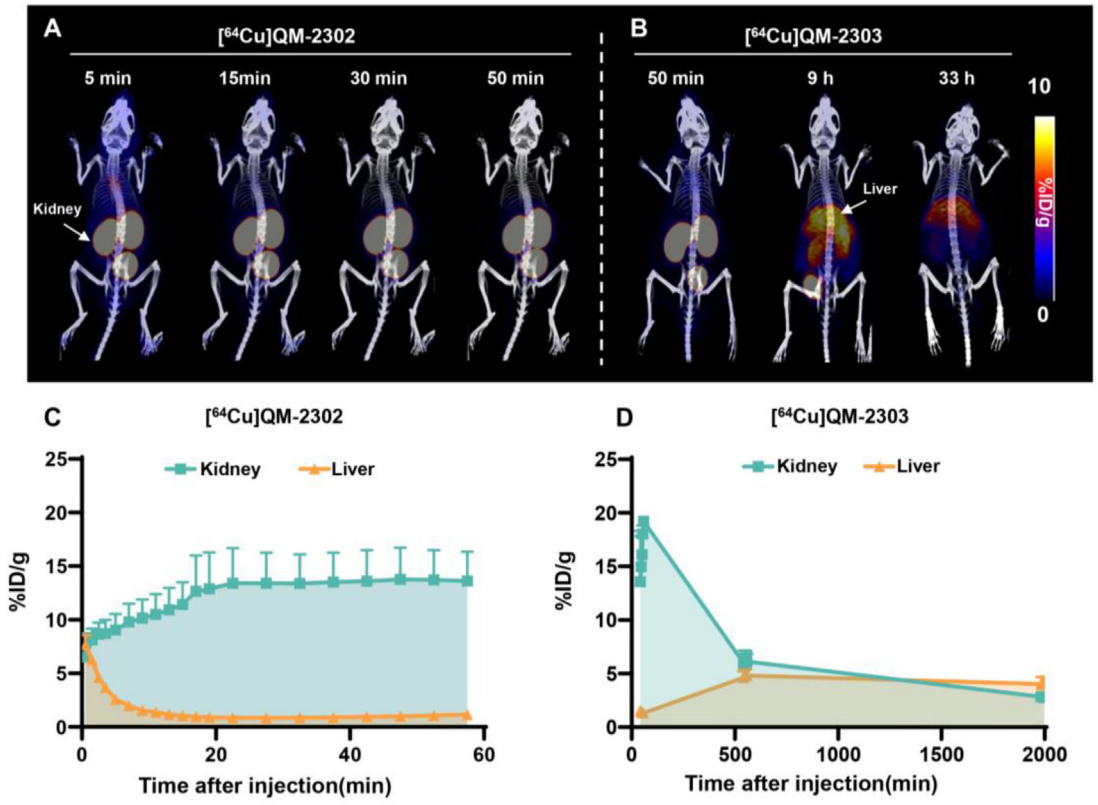

Figure 3 PET/CT imaging of [^{64}Cu]QM-2302 and [^{64}Cu]QM-2303 in healthy mice. (A, B) PET image series of [^{64}Cu]QM-2302 (A) and [^{64}Cu]QM-2303 (B) in healthy mice after injection of each radiotracer (200 μCi in 100 μL per mouse) for different time points ($n = 3$). The dashed circles indicate the kidney (green) and liver (orange). (C, D) Time−activity curves of the liver and kidney uptake calculated from dynamic PET imaging of healthy mice injected with [^{64}Cu]QM-2301 within 1 h (C) and [^{64}Cu]QM-2303 within 33 h (D). The radiotracer uptake is presented as %ID/g (the percentage of the total injected dose/per gram). All the quantitative experiments were performed independently at least three times (data are the mean ± SD, $n = 3$).

demonstrated significantly greater tumor uptake, indicating the important role of the multivalent PEGibody in improving tumor uptake and retention (Supporting Information Fig. S7A and S7C).

The *ex vivo* biodistribution of [^{64}Cu]QM-2301, [^{64}Cu]QM-2302, and [^{64}Cu]QM-2303 was determined in B16F10 tumor-bearing mice (Fig. 5A−C). Consistently, [^{64}Cu]QM-2303 exhibited higher tumor uptake at the four tested time points. The tumor accumulation of [^{64}Cu]QM-2303 was 3.40 %ID/g at 24 h p.i., which was greater than that of [^{64}Cu]QM-2301 and [^{64}Cu]QM-2302. Interestingly, no significant increase in the blood or heart accumulation of [^{64}Cu]QM-2303 was observed compared with that of non-PEGylated radioligands, demonstrating that PEGibody improved tumor uptake independent of increased blood circulation time, making it a safe modification strategy. Additionally, the tumor-to-background ratios, including the tumor-to-muscle, tumor-to-bone, tumor-to-blood, and tumor-to-liver ratios, demonstrated durable tumor retention of [^{64}Cu]QM-2303 (Fig. 5D).

IsoDGR is a small cyclic peptide composed of five amino acids that is commonly used to target integrin $\alpha5\beta1$[31]. Radiolabeled [^{99m}Tc]isoDGR has proven to be an effective tracer for monitoring integrin $\alpha5\beta1$-positive tumors[52]. To evaluate the ability of [^{64}Cu]QM-2303 to track the tumor integrin $\alpha5\beta1$, we compared its *in vivo* behavior with that of [^{64}Cu]isoDGR. PET imaging revealed comparable tumor uptake of [^{64}Cu]isoDGR at 30 min p.i (Fig. S7B and S7C). [^{64}Cu]QM-2303 exhibited greater tumor uptake than [^{64}Cu]isoDGR at 1 h p.i (Fig. S7C). The accumulation of [^{64}Cu]QM-2303 in the kidneys was significantly higher than that of [^{64}Cu]isoDGR (Fig. S7C), suggesting a different excretion profile for [^{64}Cu]isoDGR. There was no significant difference in the liver uptake of these radioligands (Fig. S7D). These data suggested that the PEGibody [^{64}Cu]QM-2303 was more effective for tumor detection than [^{64}Cu]isoDGR, but its renal toxicity requires further investigation.

3.4. *In vivo toxicity assessment of [^{64}Cu]QM-2303*

We investigated the potential toxicity of [^{64}Cu]QM-2303 *in vivo* after intravenous injection of a high dose (3 mCi per mouse) of radioligand into healthy mice. Mice treated with the same volume of saline were considered as the control group. The body weight of each mouse was measured before radioligand injection (Day −1) and at 1, 3, 7, 15, and 30 days p.i.. The results showed a gradual increase in body weight 1 month p.i., and there was no significant difference between mice treated with saline and those treated with [^{64}Cu]QM-2303 (Fig. 6A).

The radio-related toxicity of [^{64}Cu]QM-2303 was assessed through hematological analysis. The white blood cell (WBC) count slightly increased after 1 day of injection and decreased to normal (the level before radiotracer injection) from 3 to 15 days p.i. Subsequently, a significant increase in the WBC count was detected in the mice after radiotracer exposure for 30 days

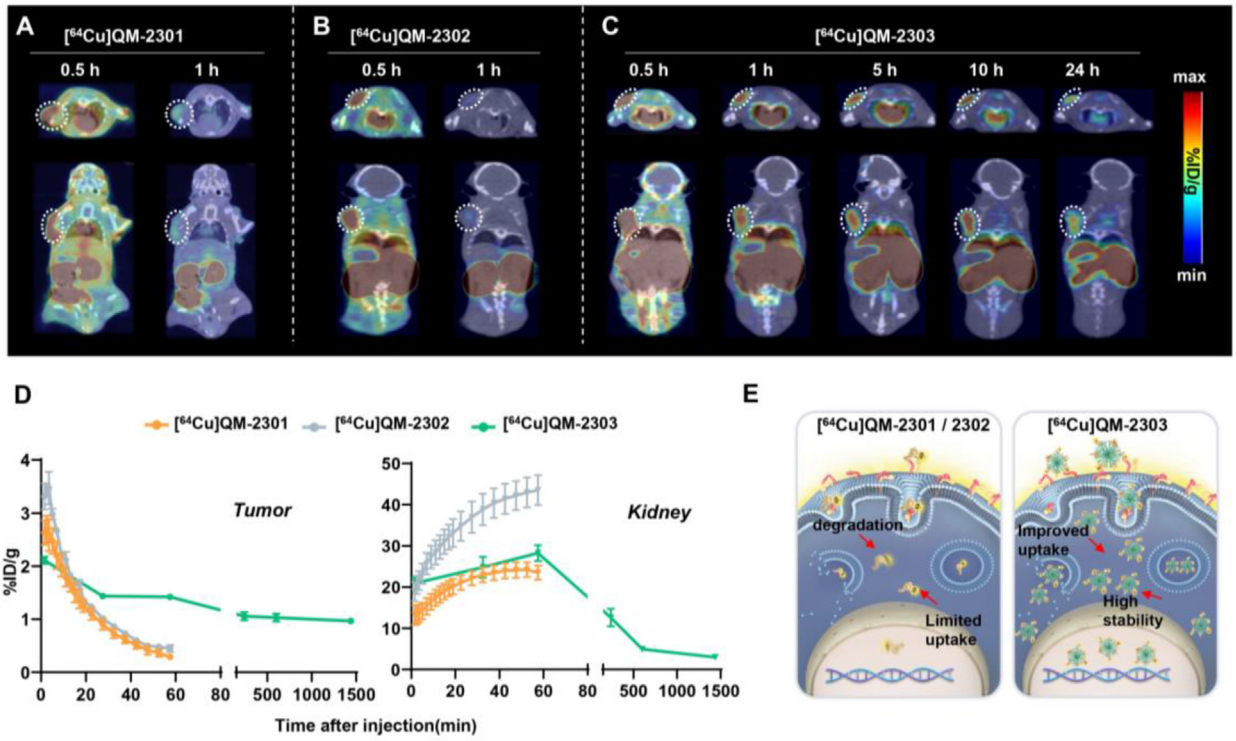

Figure 4 PET/CT imaging of [^{64}Cu]QM-2301, [^{64}Cu]QM-2302, and [^{64}Cu]QM-2303 in B16F10 tumor-bearing mice. (A−C) Series PET/CT images of [^{64}Cu]QM-2301 (A), [^{64}Cu]QM-2302 (B), and [^{64}Cu]QM-2303 (C) in B16F10 tumor-bearing mice within 1 h after injection ([^{64}Cu]QM-2301, [^{64}Cu]QM-2302) and within 24 h ([^{64}Cu]QM-2303). (D) Time−activity curves of the tumor (left) and kidney (right) uptake calculated from PET imaging of B16F10 tumor-bearing mice injected with [^{64}Cu]QM-2301 and [^{64}Cu]QM-2302 within 1 h and [^{64}Cu]QM-2303 within 24 h. (E) Schematic diagrams indicating the *in vivo* behavior of [^{64}Cu]QM-2301, [^{64}Cu]QM-2302 (left), and [^{64}Cu]QM-2303 (right). Compared with [^{64}Cu]QM-2301 and [^{64}Cu]QM-2302, [^{64}Cu]QM-2303 exhibited enhanced cell uptake and *in vivo* stability, as demonstrated by prolonged tumor accumulation and retention. All the quantitative experiments were performed independently at least three times (data are the mean ± SD, $n = 4$).

(Fig. 6B), suggesting an inflammatory response to radiation. Additionally, the red blood cell (RBC) count, hemoglobin (HGB), hematocrit (HCT), mean corpuscular volume (MCV), mean corpuscular hemoglobin (MCH), mean corpuscular hemoglobin concentration (MCHC), and platelet (PLT) counts did not significantly change after 30 days of [^{64}Cu]QM-2303 injection (Fig. 6B). Together, these results confirmed the low hematological cytotoxicity of [^{64}Cu]QM-2303, which was achieved by a relatively short blood circulation time.

After 30 days of radioligand treatment, H&E staining of the major organs was performed to determine the pathological toxicity of [^{64}Cu]QM-2303. H&E staining revealed no difference and no structural lesion in the major organs between mice treated with saline and mice treated with a high [^{64}Cu]QM-2303 dose (Fig. 6C). Despite high renal uptake and residence, no noticeable pathological change in the kidneys were observed, demonstrating considerable kidney safety (Fig. 6C).

3.5. *Anti-tumor assessment of [^{177}Lu]QM-2303*

The prolonged retention time and enhanced accumulation in tumors of [^{64}Cu]QM-2303 led us to evaluate its therapeutic efficacy in tumor-bearing mice. Lutetium-177, which has a half-life of 6.67 days, is an ideal therapeutic radionuclide for achieving antitumor effects. Therefore, QM-2303 was radiolabeled with ^{177}Lu *via* the chelator NOTA. B16F10 tumor-bearing mice were treated with a single dose of [^{177}Lu]QM-2301 or [^{177}Lu]QM-2303 (500 μCi per mouse), and the antitumor effect was assessed 28 days after single-dose injection (Fig. 7A). The [^{177}Lu]QM-2301 and [^{177}Lu]QM-2303 significantly inhibited tumor growth within 28 days, as indicated by the decreased tumor volume compared with the saline-treated group, which showed continuous tumor growth during the therapeutic study (Fig. 7B). Importantly, significantly slower tumor growth was observed in mice treated with [^{177}Lu]QM-2303 than in those treated with [^{177}Lu]QM-2301 (Fig. 7B−E). Notably, two mice subjected to saline treatment reached the endpoint on Days 22 and 24, while all mice survived after [^{177}Lu]QM-2301 and [^{177}Lu]QM-2303 treatment (Fig. 7C−E). H&E staining of the treated tumor allografts at 28 days p.i. confirmed the strong tumor-killing effects of [^{177}Lu]QM-2303 (Fig. 7I). These results demonstrated the long-term and durable antitumor efficacy of [^{177}Lu]QM-2303 in integrin $\alpha5\beta1$-positive tumors.

We also investigated the biosafety of [^{177}Lu]QM-2301 and [^{177}Lu]QM-2302 *in vivo*. Body weight was measured every 2 days and showed no significant changes throughout the experimental period (Fig. 7F). Additionally, body weight was similar among tumor-bearing mice treated with saline, [^{177}Lu]QM-2301, and [^{177}Lu]QM-2303 (Fig. 7F). We also performed hematological analysis to evaluate blood toxicity. Consistently, the WBC, RBC, HGB, HCT, MCV, MCH, MCHC, and PLT data tended to stabilize during the therapeutic process and were similar among the three experimental groups (Fig. 7G). However, a temporary decrease in WBC at 21 days p.i. was observed in mice treated with [^{177}Lu]QM-2303, which returned to normal at 28 days p.i., demonstrating

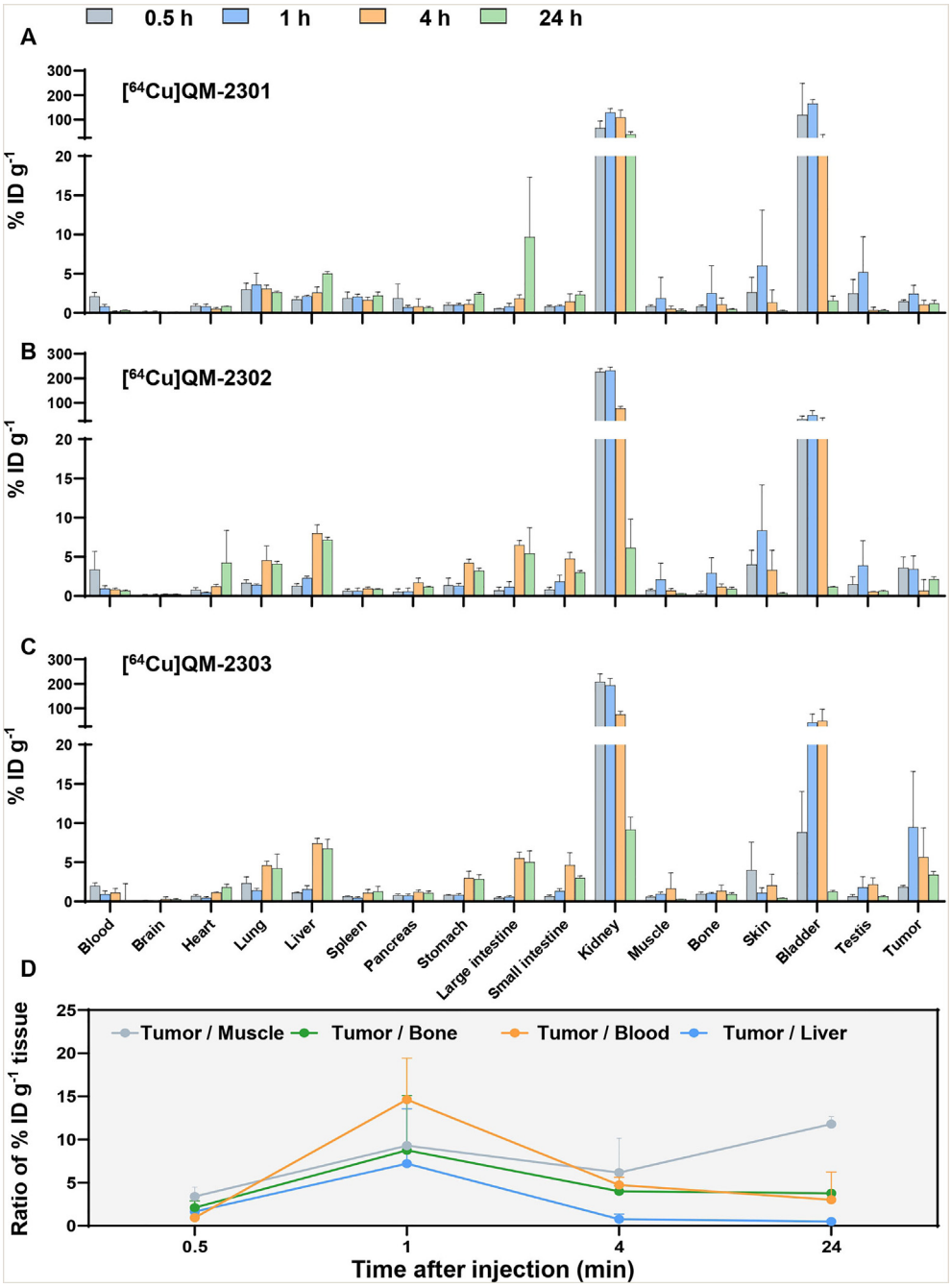

Figure 5 *Ex vivo* biodistribution of [^{64}Cu]QM-2301, [^{64}Cu]QM-2302, and [^{64}Cu]QM-2303 in B16F10 tumor-bearing mice. (A–C) Accumulation of [^{64}Cu]QM-2301, [^{64}Cu]QM-2302, and [^{64}Cu]QM-2303 in blood, tumors, and major organs determined by *ex vivo* biodistribution assay in B16F10 tumor-bearing mice. After injection of each radiotracer (200 μCi per mouse) for 0.5, 1, 4, or 24 h, B16F10 tumor-bearing mice were sacrificed (3 mice for each time point). The blood, tumor, and major organs were harvested to measure the radioactivity in the autogramma counter. (D) Tumor-to-background (muscle, bone, blood and liver) ratios of [^{64}Cu]QM-2303. The radiotracer uptake is presented as %ID/g (the percentage of the total injected dose/per gram). The values were calculated based on the *ex vivo* biodistribution data and all the quantitative experiments were performed independently at least three times (data are the mean ± SD, $n = 3$).

that [^{177}Lu]QM-2303 had fewer impact on WBC, which is consistent with previous findings[53]. Liver and kidney function, as indicated by alanine aminotransferase (ALT), aspartate aminotransferase (AST) levels, blood urea nitrogen (UREA), and creatinine (CREA) levels, were not significantly different among the saline-, [^{177}Lu]QM-2301- and [^{177}Lu]QM-2303-treated mice after 28 days of treatment (Fig. 7H). Moreover, H&E staining of the heart, liver, spleen, lung and kidney of tumor-bearing mice revealed no noticeable histological or structural lesions at 28 days after saline, [^{177}Lu]QM-2301 or [^{177}Lu]QM-2303 administration (Fig. 7I). Together, these results demonstrated that the [^{177}Lu]QM-2303-based TRT modality had low toxicity and good safety.

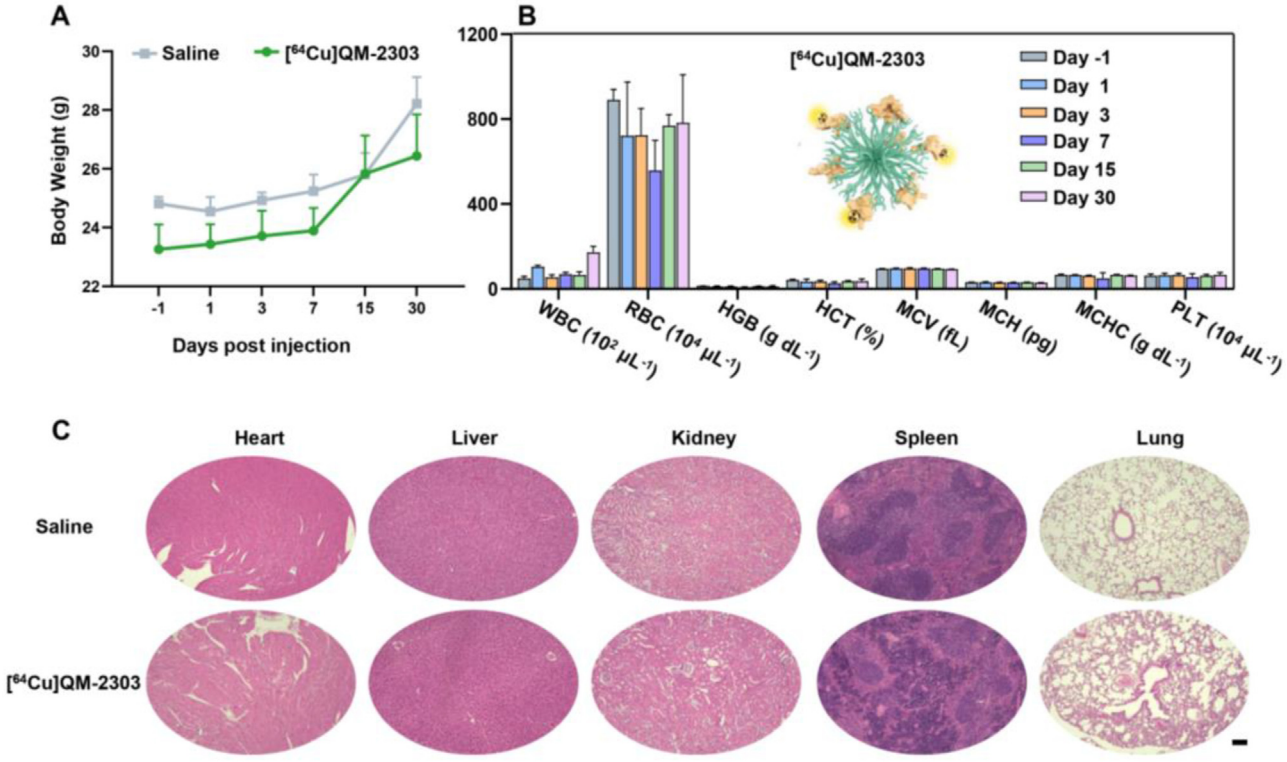

Figure 6 *In vivo* toxicity assessment of [^{64}Cu]QM-2303 in healthy mice. (A) Body weight changes in healthy mice before and after saline or [^{64}Cu]QM-2303 (3 mCi per mouse) injection for 30 days. (B) Hematological analysis of mice before and after [^{64}Cu]QM-2303 injection. The WBC, RBC, HGB, HCT, MCV, MCH, MCHC, and PLT counts are presented. Body weight and hematological parameters were measured at 1, 3, 7, 15, and 30 days p.i. Day −1 indicated one day before the injection of the radiotracer. (C) H&E staining images of the heart, liver, kidney, spleen, and lung of mice treated with saline and [^{64}Cu]QM-2303 at 30 days p.i., indicating no apparent organ damage. All the quantitative experiments were performed independently at least three times (data are the mean ± SD, $n = 3$).

4. Discussion

In this study, we developed a PEGibody-based radiopharmaceuticals, [^{64}Cu]/[^{177}Lu]QM-2303, which demonstrated satisfactory binding affinity, tumor retention time and antitumor effects. Our results confirmed the formation of a PEGibody ([^{64}Cu]QM-2303) with a diameter between 100 and 200 nm. After incubation with murine serum for 1 h, more than 80% of [^{64}Cu]QM-2303 remained intact, while [^{64}Cu]QM-2301 and [^{64}Cu]QM-2302 mostly degraded, indicating the superior stability of [^{64}Cu]QM-2303. *In vitro* SPR measurements, cell uptake assays, and competitive inhibition assays also confirmed its greater binding affinity to integrin $\alpha5\beta1$. PEGibody formation prevented the degradation of radiotracers and increased the number of binding sites available on integrin $\alpha5\beta1$ for the radiotracers, enhancing the tumor uptake and stability of the PEGibody. Additionally, the formation of the PEGibody-based radiotracer [^{64}Cu]QM-2303 was based on the PEGylated peptides themselves, without other nanoparticles, such as liposomes[35], making it a safe and available radiotracer in clinical practice.

The promoted *in vitro* stability and cell uptake of [^{64}Cu]QM-2303 suggested improved *in vitro* performance. Considering potential issues, including slow excretion and cytotoxicity caused by the large molecular weight of [^{64}Cu]QM-2303, we analyzed its pharmacokinetic property *in vivo*, which revealed rapid blood clearance and renal excretion of [^{64}Cu]QM-2303. Body weight assessment, hematological analysis and pathological analysis were performed after the administration of a high dose (3 mCi per mouse) of [^{64}Cu]QM-2303. The data revealed no evident toxicity in the whole body, blood or major organs, especially in the liver or kidneys, with high accumulation and prolonged retention time of [^{64}Cu]QM-2303. Taken together, these results demonstrate the safety of PEGibody-based radiotracers for tumor integrin $\alpha5\beta1$ imaging.

PET/CT imaging and *ex vivo* biodistribution in B16F10 tumor-bearing mice showed prolonged tumor retention time of [^{64}Cu]QM-2303. The tumor accumulation of [^{64}Cu]QM-2303 stabilized from 1 h to 24 h p.i., whereas a weak signal was observed for [^{64}Cu]QM-2301 and [^{64}Cu]QM-2302 at the tumor site after 1 h p.i. Notably, PEGibody did not extend the peptides' circulation time in the bloodstream, as indicated by the blood and heart accumulation of [^{64}Cu]QM-2303, which was different from conventional peptide modification strategies. Therefore, PEGibody improved the tumor uptake and retention time of radiotracers without increasing concerns about hematological toxicity. Improved tumor uptake and accumulation were achieved by multiple binding sites of PEGibody, a high binding capacity, and enhanced stability. Additionally, the enhanced permeability and retention effect of the tumor tissue may also have contributed to improved tumor uptake, characterized by the increased accumulation of macromolecules, such as PEGibody. In addition, PEG molecules self-assembled to form a PEGibody with PEG molecules in the center and the targeted peptide on the surface. The hiding of PEG chains in the PEGibody reduces the binding of PEG molecules to proteins in the blood, which is the common mechanism of conventional PEGylation strategy to prolong the blood

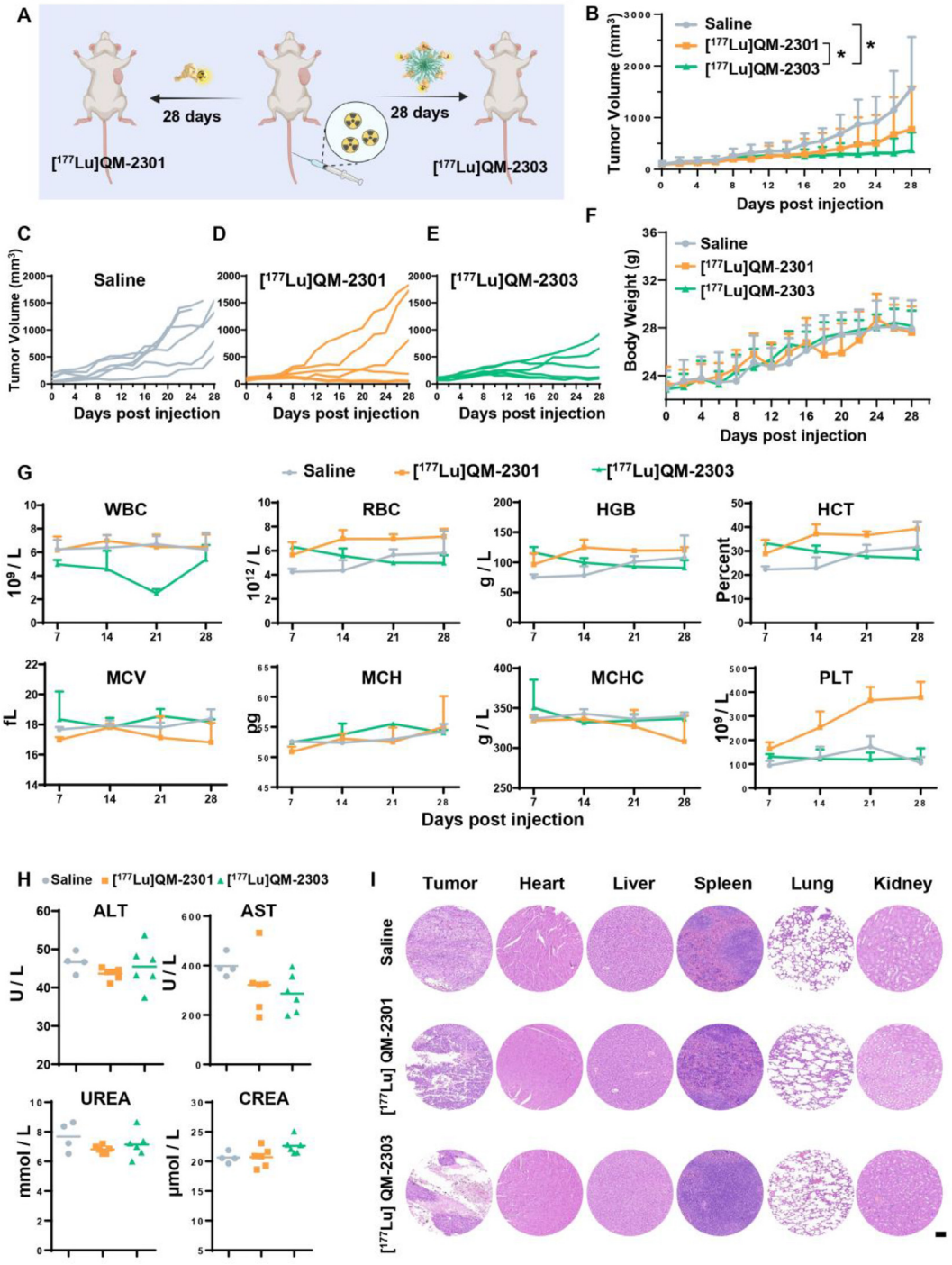

Figure 7 *In vivo* antitumor efficacy of [^{177}Lu]QM-2303 in B16F10 tumor-bearing mice. (A) Illustration of the antitumor experiments. A single dose of [^{177}Lu]QM-2301 (500 μCi), [^{177}Lu]QM-2303 (500 μCi) or saline (control) was injected into B16F10 tumor-bearing mice. All mice were sacrificed after 28 days ($n = 6$). The tumor size and body weight were measured every 2 days. (B−E) Tumor volume and tumor growth of mice during 28 days of therapy, shown as the mean tumor size (B) and the tumor volume of individual mice in each group (C−E). (F) Changes in body weight of mice treated with saline, [^{177}Lu]QM-2301, or [^{177}Lu]QM-2303 for 28 days. (G) Hematological analysis showing the WBC, RBC, HGB, HCT, MCV, MCH, MCHC, and PLT levels of mice after drug administration for 28 days. (H) The liver (ALT, AST) and kidney (UREA, CREA) function of mice treated with saline, [^{177}Lu]QM-2301, or [^{177}Lu]QM-2303 at 28 days p.i.. (I) H&E staining images of the tumor, heart, liver, kidney, spleen and lung in mice treated with saline, [^{177}Lu]QM-2301, and [^{177}Lu]QM-2303 at 28 days p.i. The scale bar indicates 100 μm. All the quantitative experiments were performed independently at least three times (data are the mean ± SD, $n = 6$). *$P < 0.05$.

circulation time of compounds. Therefore, PEGibody could serve as a safe and robust platform for chemical modification. Furthermore, [^{64}Cu]QM-2303 exhibited better tumor uptake than [^{64}Cu]isoDGR. These promising results suggest that [^{64}Cu]QM-2303 could bridge the gap between basic research and clinical application, warranting a first-in-human study. Future studies should focus on expanding the application of [^{64}Cu]QM-2303 in cancer research using multiple tumor models to evaluate its efficacy in cancers overexpressing integrin $\alpha5\beta1$.

Finally, the therapeutic potential of [^{177}Lu]QM-2303 in B16F10 tumor-bearing mice was evaluated. Compared with [^{177}Lu]QM-2301, [^{177}Lu]QM-2303 showed robust antitumor efficacy, as indicated by significantly reduced tumor growth. Considering the increased liver uptake of [^{64}Cu]QM-2303, we also investigated the *in vivo* toxicity of [^{177}Lu]QM-2303 in tumor-bearing mice. [^{177}Lu]QM-2303, which consistent of [^{64}Cu]QM-2303, caused no significant injury to the major organs or blood, which further confirmed the satisfactory blood circulation time and reduced our concern about the biosafety of [^{177}Lu]QM-2303. Therefore, [^{177}Lu]QM-2303-based treatment is a safe targeted therapeutic modality that has remarkable clinical potential for the treatment of integrin $\alpha5\beta1$-positive tumors.

5. Conclusions

This study reported a novel method for generating a PEGylation-enabled peptide multidisplay platform through PEGylation and self-assembly, denoted as PEGibody-based radiopharmaceuticals. With this method, we prepared an integrin $\alpha5\beta1$-targeted PEGibody, namely, [^{64}Cu]/[^{177}Lu]QM-2303, and demonstrated its advantages in enhancing stability, binding affinity, tumor retention, and antitumor efficacy without expanding circulation time in the bloodstream, providing potential radiotheranostics for patients with integrin $\alpha5\beta1$ overexpressed cancers without causing hematological or organ toxicity. Therefore, PEGibody-based radiopharmaceuticals hold promise for the potential translation of integrin $\alpha5\beta1$ tumor tracers from the realm of basic research to practical clinical applications.

Acknowledgments

This study was supported by the National Natural Science Foundation of China (No. 82372002), the Nonprofit Central Research Institute Fund of the Chinese Academy of Medical Sciences (No. 2022-RC350-04, China), the CAMS Innovation Fund for Medical Sciences (Nos. 2021-I2M-1−026 (2023), 2022-I2M-2-002-2, and 2021-I2M-3-001 (2023), China), the National Key Research and Development Program of China (No. 2022YFE0111700), and the Beijing Nova Program to Kuan Hu (No. 0104002, China). This work was also supported by the Beijing Natural Science Foundation (No. L234044, China), the Fundamental Research Funds for the Central Universities (Nos. 3332023044 and 3332023151, China), the CIRP Open Fund of Radiation Protection Laboratories (No. ZHYLYB2021005, China), and the China National Nuclear Corporation Young Talent Program.

Author contributions

Siqi Zhang: Data curation, Formal analysis, Funding acquisition, Writing − original draft, Writing − review & editing. Xiaohui Ma: Conceptualization, Formal analysis, Investigation, Writing − original draft, Writing − review & editing. Jiang Wu: Data curation, Formal analysis, Methodology. Jieting Shen: Data curation, Formal analysis, Software, Writing − review & editing. Yuntao Shi: Data curation, Formal analysis, Software. Xingkai Wang: Formal analysis, Methodology, Writing − review & editing. Lin Xie: Investigation, Methodology. Xiaona Sun: Formal analysis, Writing − review & editing. Yuxuan Wu: Data curation, Writing − review & editing. Hao Tian: Writing − review & editing. Xin Gao: Formal analysis. Xueyao Chen: Data curation. Hongyi Huang: Formal analysis, Software. Lu Chen: Formal analysis. Xuekai Song: Writing − review & editing. Qichen Hu: Writing − review & editing. Hailong Zhang: Conceptualization. Feng Wang: Conceptualization, Funding acquisition, Investigation. Zhao-Hui Jin: Conceptualization, Data curation, Formal analysis, Investigation, Supervision, Writing − review & editing. Ming-Rong Zhang: Conceptualization, Data curation, Formal analysis, Software, Writing − review & editing. Rui Wang: Conceptualization, Project administration, Supervision, Writing − review & editing. Kuan Hu: Conceptualization, Data curation, Formal analysis, Supervision, Writing − original draft, Writing − review & editing.

Conflicts of interest

The authors declare no conflicts of interest.

Appendix A. Supporting information

Supporting information to this article can be found online at https://doi.org/10.1016/j.apsb.2024.07.006.

References

1. Aboagye EO, Barwick TD, Haberkorn U. Radiotheranostics in oncology: making precision medicine possible. *CA Cancer J Clin* 2023;**73**:255−74.
2. Bodei L, Herrmann K, Schoder H, Scott AM, Lewis J. Radiotheranostics in oncology: current challenges and emerging opportunities. *Nat Rev Clin Oncol* 2022;**19**:534−50.
3. Boros E, Packard AB. Radioactive transition metals for imaging and therapy. *Chem Rev* 2018;**119**:870−901.
4. Dolgin E. Radioactive drugs emerge from the shadows to storm the market. *Nat Biotechnol* 2018;**36**:1125−7.
5. Sgouros G, Bodei L, McDevitt MR, Nedrow JR. Radiopharmaceutical therapy in cancer: clinical advances and challenges. *Nat Rev Drug Discov* 2020;**19**:589−608.
6. Hu K, Li J, Wang L, Huang Y, Li L, Ye S, et al. Preclinical evaluation and pilot clinical study of [^{18}F]AlF-labeled FAPI-tracer for PET imaging of cancer associated fibroblasts. *Acta Pharm Sin B* 2022;**12**:867−75.
7. Craik DJ, Fairlie DP, Liras S, Price D. The future of peptide-based drugs. *Chem Biol Drug Des* 2013;**81**:136−47.
8. Cooper BM, Iegre J, Dh OD, Olwegard Halvarsson M, Spring DR. Peptides as a platform for targeted therapeutics for cancer: peptide−drug conjugates (PDCs). *Chem Soc Rev* 2021;**50**:1480−94.
9. Bodei L, Kwekkeboom DJ, Kidd M, Modlin IM, Krenning EP. Radiolabeled somatostatin analogue therapy of gastroenteropancreatic cancer. *Semin Nucl Med* 2016;**46**:225−38.
10. Bodei L, Kidd M, Paganelli G, Grana CM, Drozdov I, Cremonesi M, et al. Long-term tolerability of PRRT in 807 patients with neuroendocrine tumours: the value and limitations of clinical factors. *Eur J Nucl Med Mol Imaging* 2015;**42**:5−19.
11. Schuchardt C, Zhang J, Kulkarni HR, Chen X, Muller D, Baum RP. Prostate-specific membrane antigen radioligand therapy using ^{177}Lu-

PSMA I&T and ^{177}Lu-PSMA-617 in patients with metastatic castration-resistant prostate cancer: comparison of safety, biodistribution, and dosimetry. *J Nucl Med* 2022;**63**:1199−207.
12. Hofman MS, Violet J, Hicks RJ, Ferdinandus J, Thang SP, Akhurst T, et al. [^{177}Lu]-PSMA-617 radionuclide treatment in patients with metastatic castration-resistant prostate cancer (LuPSMA trial): a single-centre, single-arm, phase 2 study. *Lancet Oncol* 2018;**19**:825−33.
13. Kuten J, Fahoum I, Savin Z, Shamni O, Gitstein G, Hershkovitz D, et al. Head-to-head comparison of ^{68}Ga-PSMA-11 with ^{18}F-PSMA-1007 PET/CT in staging prostate cancer using histopathology and immunohistochemical analysis as a reference standard. *J Nucl Med* 2020;**61**:527−32.
14. Hope TA, Eiber M, Armstrong WR, Juarez R, Murthy V, Lawhn-Heath C, et al. Diagnostic accuracy of ^{68}Ga-PSMA-11 PET for pelvic nodal metastasis detection prior to radical prostatectomy and pelvic lymph node dissection: a multicenter prospective phase 3 imaging trial. *JAMA Oncol* 2021;**7**:1635−42.
15. Rodnick ME, Sollert C, Stark D, Clark M, Katsifis A, Hockley BG, et al. Synthesis of ^{68}Ga-radiopharmaceuticals using both generator-derived and cyclotron-produced ^{68}Ga as exemplified by [^{68}Ga]Ga-PSMA-11 for prostate cancer PET imaging. *Nat Protoc* 2022;**17**:980−1003.
16. Gill MR, Falzone N, Du Y, Vallis KA. Targeted radionuclide therapy in combined-modality regimens. *Lancet Oncol* 2017;**18**:e414−23.
17. Alati S, Singh R, Pomper MG, Rowe SP, Banerjee SR. Preclinical development in radiopharmaceutical therapy for prostate cancer. *Semin Nucl Med* 2023;**53**:663−86.
18. Salerno KE, Roy S, Ribaudo C, Fisher T, Patel RB, Mena E, et al. A primer on radiopharmaceutical therapy. *Int J Radiat Oncol Biol Phys* 2023;**115**:48−59.
19. Paolillo M, Serra M, Schinelli S. Integrins in glioblastoma: still an attractive target?. *Pharmacol Res* 2016;**113**:55−61.
20. Renner G, Janouskova H, Noulet F, Koenig V, Guerin E, Bar S, et al. Integrin alpha5beta1 and p53 convergent pathways in the control of anti-apoptotic proteins PEA-15 and survivin in high-grade glioma. *Cell Death Differ* 2016;**23**:640−53.
21. Dudvarski Stankovic N, Bicker F, Keller S, Jones DT, Harter PN, Kienzle A, et al. EGFL7 enhances surface expression of integrin alpha5beta1 to promote angiogenesis in malignant brain tumors. *EMBO Mol Med* 2018;**10**:e8420.
22. Ninsontia C, Pongrakhananon V, Chaotham C, Chanvorachote P. Ouabain inhibits anchorage-independent growth in human lung cancer cells *via* integrin $\alpha v\beta3$ reduction. *Asian J Pharm Sci* 2016;**11**:189−90.
23. Li M, Wang Y, Li M, Wu X, Setrerrahmane S, Xu H. Integrins as attractive targets for cancer therapeutics. *Acta Pharm Sin B* 2021;**11**:2726−37.
24. Steiger K, Quigley NG, Groll T, Richter F, Zierke MA, Beer AJ, et al. There is a world beyond alphavbeta3-integrin: multimeric ligands for imaging of the integrin subtypes alphavbeta6, alphavbeta8, alphavbeta3, and alpha5beta1 by positron emission tomography. *EJNMMI Res* 2021;**11**:106.
25. Hou J, Yan D, Liu Y, Huang P, Cui H. The roles of integrin alpha5-beta1 in human cancer. *Onco Targets Ther* 2020;**13**:13329−44.
26. Li NF, Gemenetzidis E, Marshall FJ, Davies D, Yu Y, Frese K, et al. RhoC interacts with integrin alpha5beta1 and enhances its trafficking in migrating pancreatic carcinoma cells. *PLoS One* 2013;**8**:e81575.
27. Slack RJ, Macdonald SJF, Roper JA, Jenkins RG, Hatley RJD. Emerging therapeutic opportunities for integrin inhibitors. *Nat Rev Drug Discov* 2021;**21**:60−78.
28. Hamidi H, Ivaska J. Every step of the way: integrins in cancer progression and metastasis. *Nat Rev Cancer* 2018;**18**:533−48.
29. Janouskova H, Maglott A, Leger DY, Bossert C, Noulet F, Guerin E, et al. Integrin alpha5beta1 plays a critical role in resistance to temozolomide by interfering with the p53 pathway in high-grade glioma. *Cancer Res* 2012;**72**:3463−70.
30. Neubauer S, Rechenmacher F, Beer AJ, Curnis F, Pohle K, D'Alessandria C, et al. Selective imaging of the angiogenic relevant integrins $\alpha5\beta1$ and $\alpha v\beta3$. *Angew Chem-int Edit* 2013;**52**:11656−9.
31. Kapp TG, Di Leva FS, Notni J, Räder AFB, Fottner M, Reichart F, et al. *N*-Methylation of isoDGR peptides: discovery of a selective $\alpha5\beta1$-integrin ligand as a potent tumor imaging agent. *J Med Chem* 2018;**61**:2490−9.
32. Notni J, Steiger K, Hoffmann F, Reich D, Kapp TG, Rechenmacher F, et al. Complementary, selective PET imaging of integrin subtypes $\alpha5\beta1$ and $\alpha v\beta3$ using ^{68}Ga-Aquibeprin and ^{68}Ga-Avebetrin. *J Nucl Med* 2016;**57**:460−6.
33. Notni J, Steiger K, Hoffmann F, Reich D, Schwaiger M, Kessler H, et al. Variation of specific activities of ^{68}Ga-Aquibeprin and ^{68}Ga-Avebetrin enables selective PET imaging of different expression levels of integrins $\alpha5\beta1$ and $\alpha v\beta3$. *J Nucl Med* 2016;**57**:1618−24.
34. Mardilovich A, Craig JA, McCammon MQ, Garg A, Kokkoli E. Design of a novel fibronectin-mimetic peptide−amphiphile for functionalized biomaterials. *Langmuir* 2006;**22**:3259−64.
35. Shroff K, Kokkoli E. PEGylated liposomal doxorubicin targeted to $\alpha5\beta1$-expressing MDA-MB-231 breast cancer cells. *Langmuir* 2012;**28**:4729−36.
36. Shroff K, Pearce TR, Kokkoli E. Enhanced integrin mediated signaling and cell cycle progression on fibronectin mimetic peptide amphiphile monolayers. *Langmuir* 2012;**28**:1858−65.
37. Craig JA, Rexeisen EL, Mardilovich A, Shroff K, Kokkoli E. Effect of linker and spacer on the design of a fibronectin-mimetic peptide evaluated *via* cell studies and AFM adhesion forces. *Langmuir* 2008;**24**:10282−92.
38. Leahy DJ, Aukhil I, Erickson HP. Crystal structure of a four-domain segment of human fibronectin encompassing the RGD loop and synergy region. *Cell* 1996;**84**:155−64.
39. Schumacher S, Dedden D, Nunez RV, Matoba K, Takagi J, Biertümpfel C, et al. Structural insights into integrin $\alpha5\beta1$ opening by fibronectin ligand. *Sci Adv* 2021;**7**:eabe9716.
40. Hynes RO. Integrins: bidirectional, allosteric signaling machines. *Cell* 2002;**110**:673−87.
41. Jin ZH, Furukawa T, Kumata K, Xie L, Yui J, Wakizaka H, et al. Development of the fibronectin−mimetic peptide KSSPHSRN (SG) 5RGDSP as a novel radioprobe for molecular imaging of the cancer biomarker $\alpha5\beta1$ integrin. *Biol Pharm Bull* 2015;**38**:1722−31.
42. Chen X, Park R, Shahinian AH, Bading JR, Conti PS. Pharmacokinetics and tumor retention of ^{125}I-labeled RGD peptide are improved by PEGylation. *Nucl Med Biol* 2004;**31**:11−9.
43. Harris JM, Chess RB. Effect of pegylation on pharmaceuticals. *Nat Rev Drug Discov* 2003;**2**:214−21.
44. Fan X, Wang X, Li Z, Li Y. ^{68}Ga-Labeled TMTP1 derivatives with moderate hydrophilicity for positron emission tomography of hepatocellular carcinoma in high contrast. *J Med Chem* 2023;**66**:6756−65.
45. Roberts MJ, Bentley MD, Harris JM. Chemistry for peptide and protein PEGylation. *Adv Drug Deliv Rev* 2002;**54**:459−76.
46. Li L, Shang B, Hu L, Shao R, Zhen Y. Site-specific PEGylation of lidamycin and its antitumor activity. *Acta Pharm Sin B* 2015;**5**:264−9.
47. Meudom R, Zhang Y, VandenBerg MA, Zou L, Zhang YW, Webber MJ, et al. Supramolecular approaches for insulin stabilization without prolonged duration of action. *Acta Pharm Sin B* 2023;**13**:2281−90.
48. Verhoef JJF, Anchordoquy TJ. Questioning the use of PEGylation for drug delivery. *Drug Deliv Transl Res* 2013;**3**:499−503.
49. Hu K, Wu W, Xie L, Geng H, Zhang Y, Hanyu M, et al. Whole-body PET tracking of a D-dodecapeptide and its radiotheranostic potential for PD-L1 overexpressing tumors. *Acta Pharm Sin B* 2022;**12**:1363−76.
50. Hu K, Hanyu M, Xie L, Zhang YD, Nagatsu K, Suzuki H, et al. Developing native peptide-based radiotracers for PD-L1 PET imaging and improving imaging contrast by pegylation (vol 55, pg 4162, 2019). *Chem Commun* 2019;**55**:4162−5.
51. Benešová M, Schäfer M, Bauder-Wüst U, Afshar-Oromieh A, Kratochwil C, Mier W, et al. Preclinical evaluation of a tailor-made DOTA-conjugated PSMA inhibitor with optimized linker moiety for imaging and endoradiotherapy of prostate cancer. *J Nucl Med* 2015;**56**:914−20.

52. Gao H, Luo C, Yang G, Du S, Li X, Zhao H, et al. Improved in vivo targeting capability and pharmacokinetics of 99mTc-Labeled isoDGR by dimerization and albumin-binding for glioma imaging. *Bioconjug Chem* 2019;**30**:2038−48.

53. Xie L, Zhang L, Hu K, Hanyu M, Zhang Y, Fujinaga M, et al. A ^{211}At-labelled mGluR1 inhibitor induces cancer senescence to elicit long-lasting anti-tumor efficacy. *Cell Rep Med* 2023;**4**: 100960.